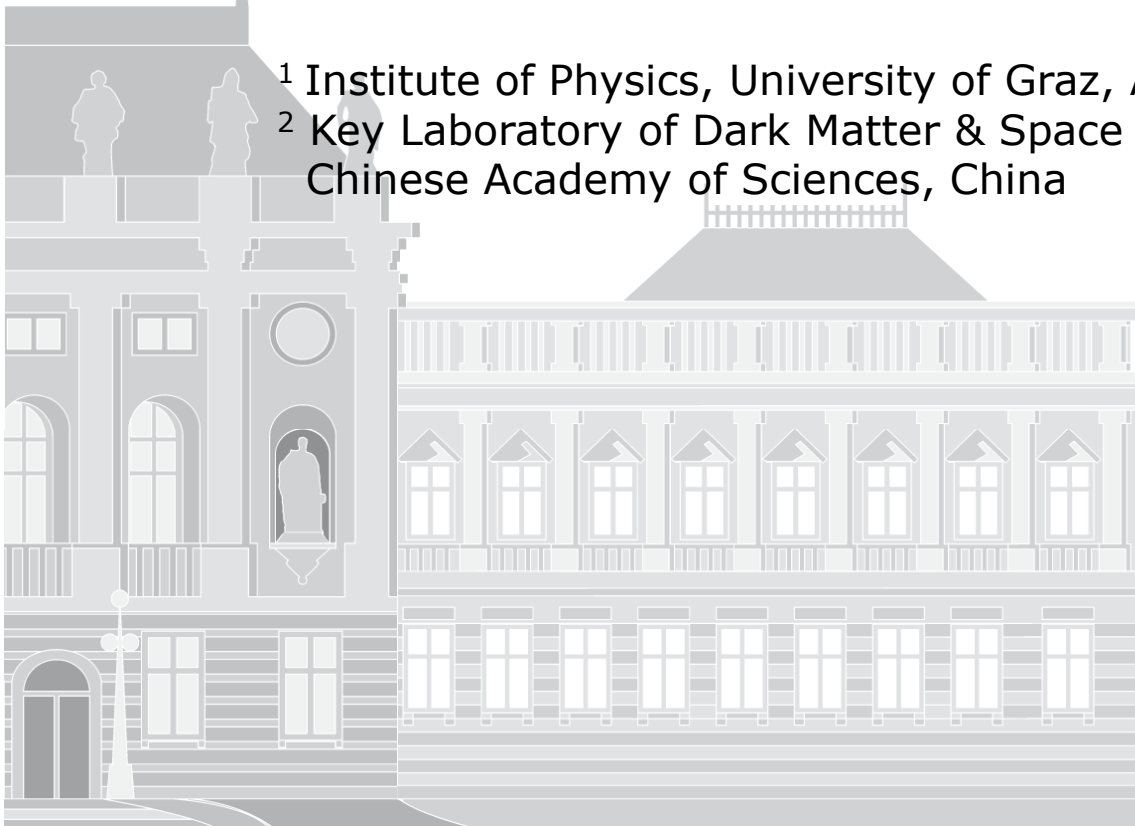


Temporal and spatial relationship of flare signatures and the coronal magnetic field

J. K. Thalmann¹, A. M. Veronig¹ & Y. Su²

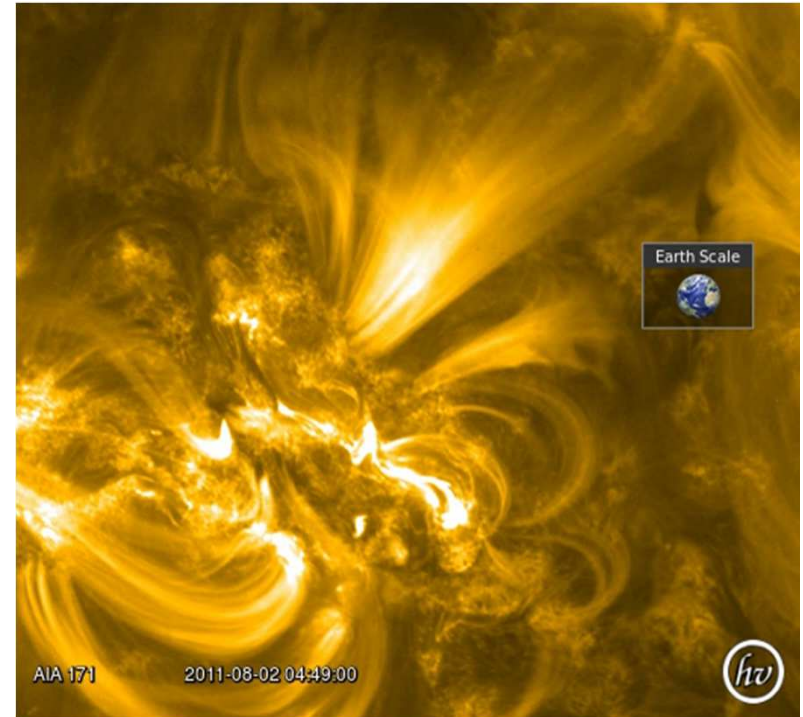
¹ Institute of Physics, University of Graz, Austria

² Key Laboratory of Dark Matter & Space Astronomy, Purple Mountain Observatory,
Chinese Academy of Sciences, China

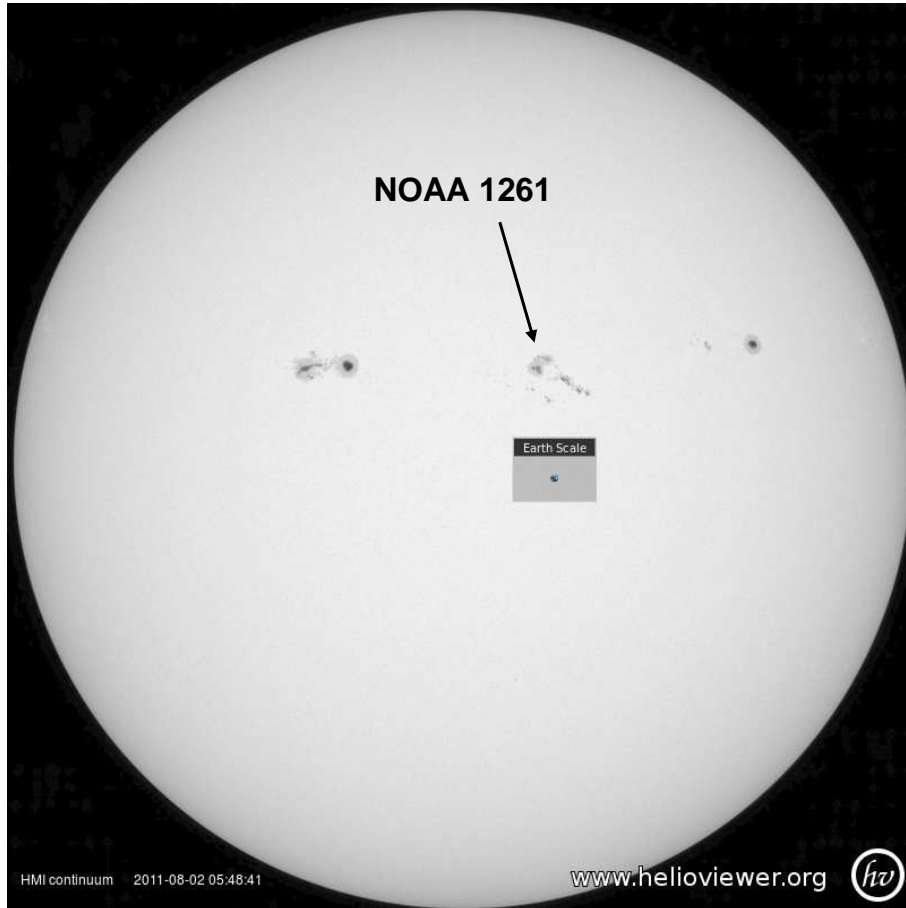


Event overview – The M(onkey) 1.6 flare

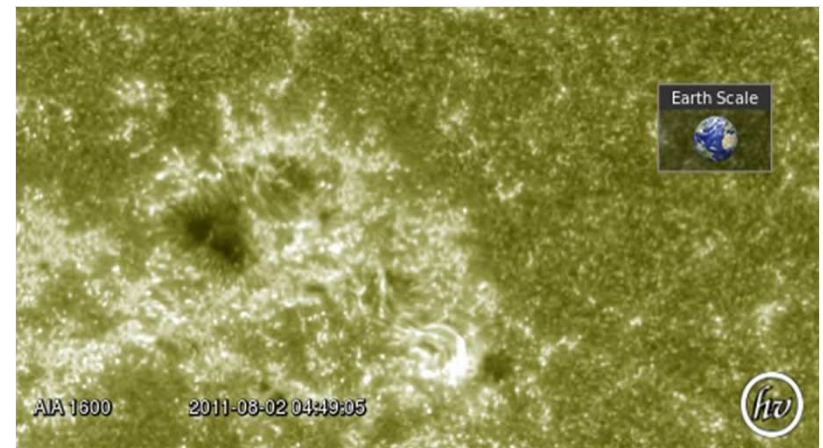
coronal emission (AIA 171 Å)



photospheric continuum emission (HMI 6173 Å)

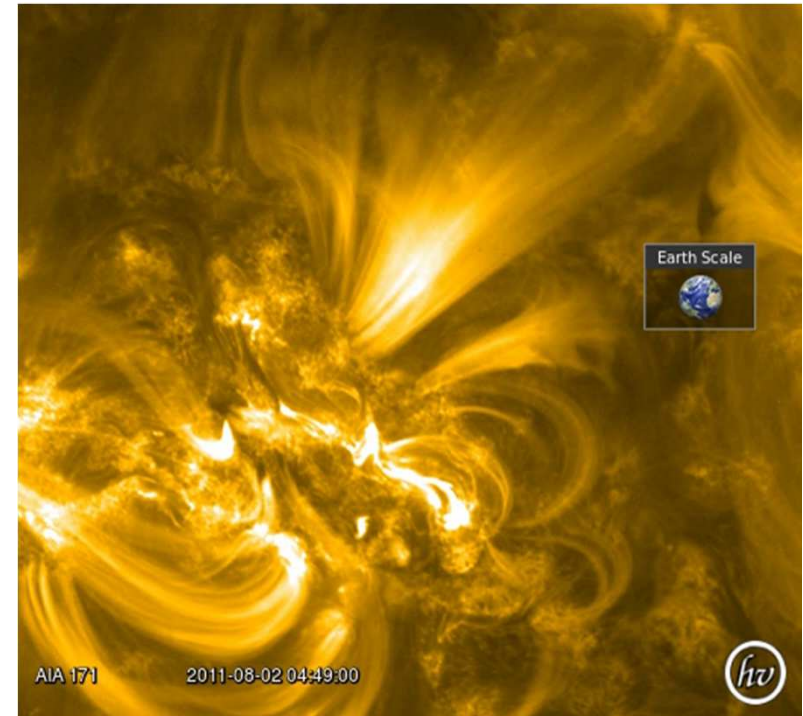


photosphere & transition region emission (AIA 1600 Å)

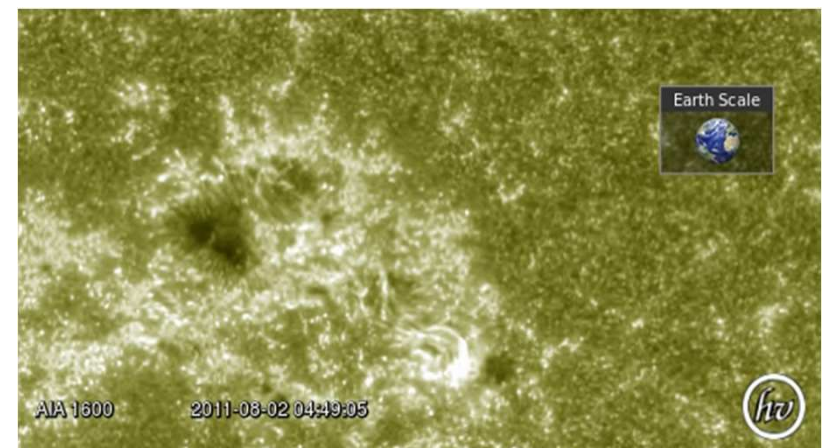


Event overview – The M(onkey) 1.6 flare

coronal emission (AIA 171 Å)

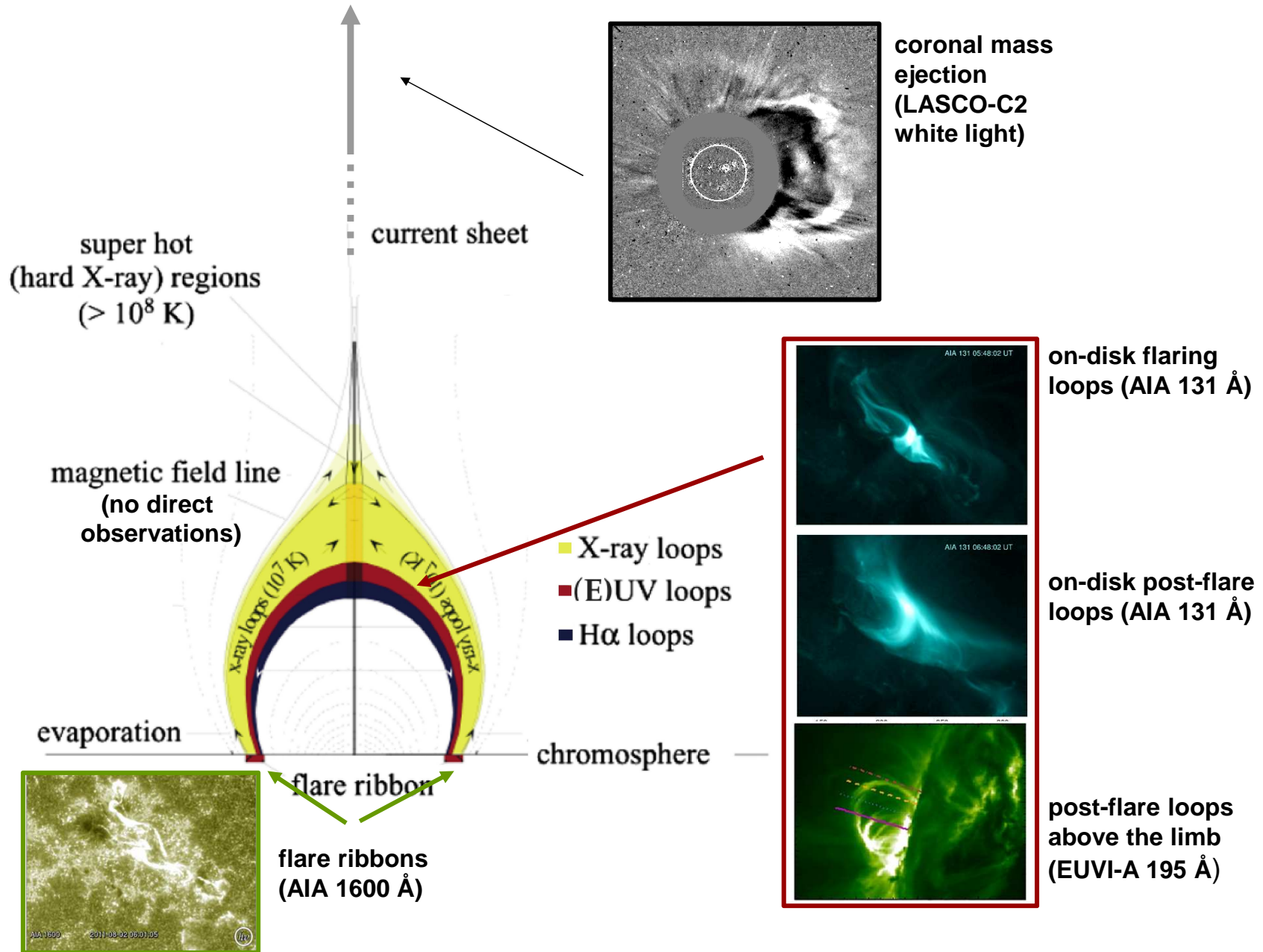


photosphere & transition region emission (AIA 1600 Å)



Event overview – The M(onkey) 1.6 flare

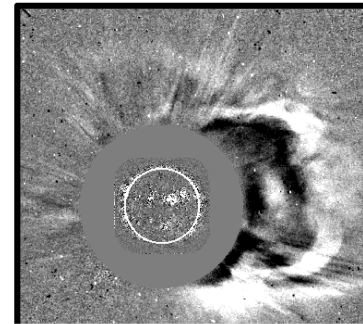
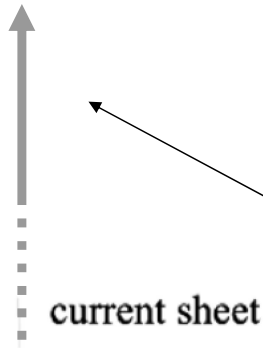
Adapted from Lin & Murphy et al., 2015, Space Sci. Rev., 194, 237.



Event overview – The M(onkey) 1.6 flare

4, 237.

super hot



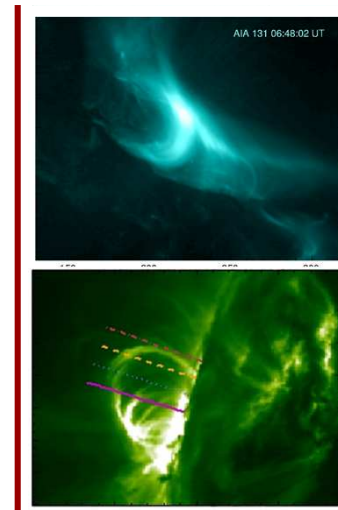
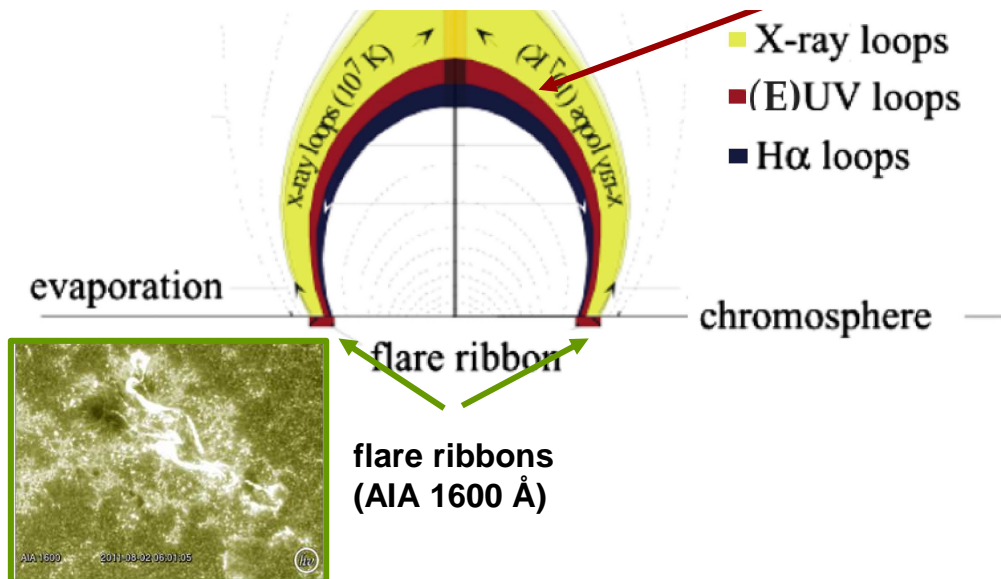
coronal mass ejection (LASCO-C2 white light)

Motivation:

How does the timing and location of the different flare-related observations compare?

What can we say about the involved coronal magnetic field?

Adapted from Lin & Murphy

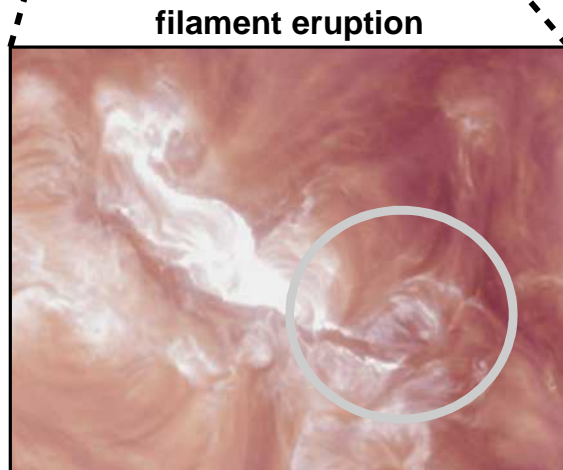
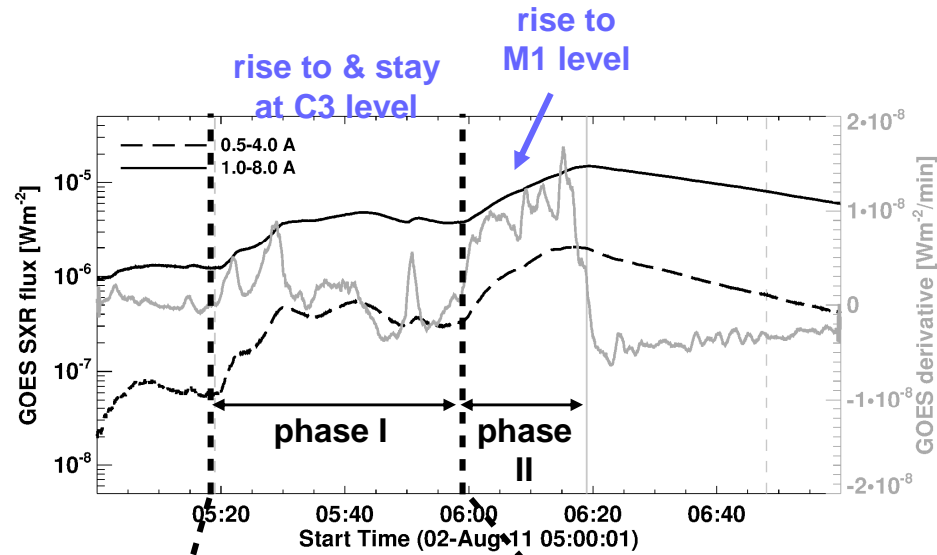


on-disk post-flare loops (AIA 131 Å)

post-flare loops above the limb (EUVI-A 195 Å)

Event overview – The M(onkey) 1.6 flare

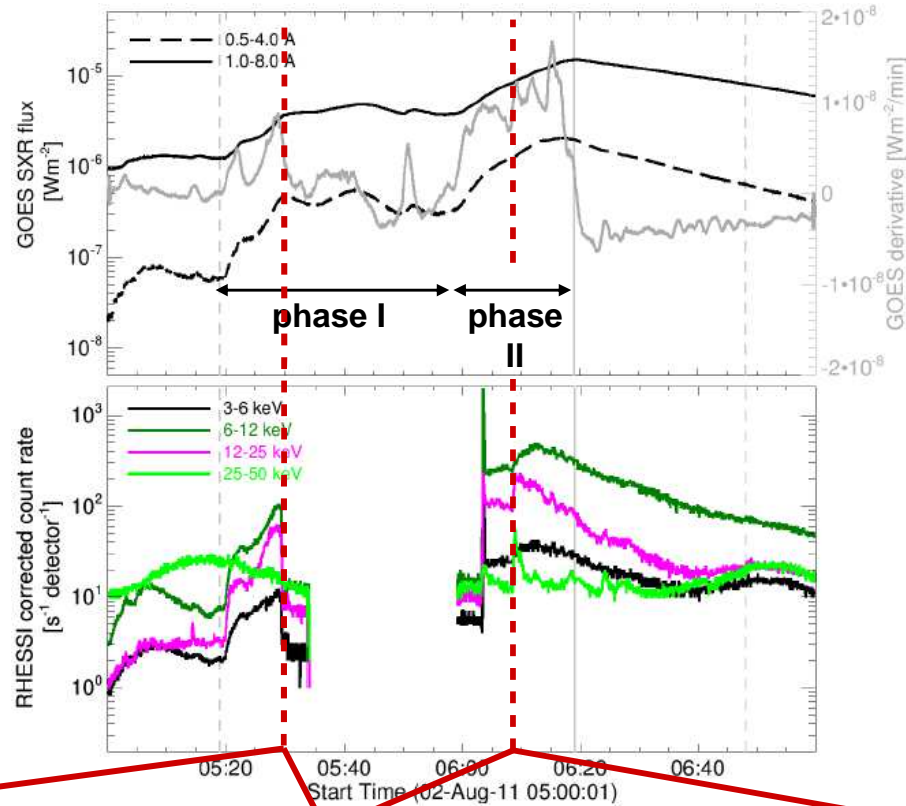
Coronal emission (AIA 171 Å)



Upper photosphere & transition region emission (AIA 1600 Å)

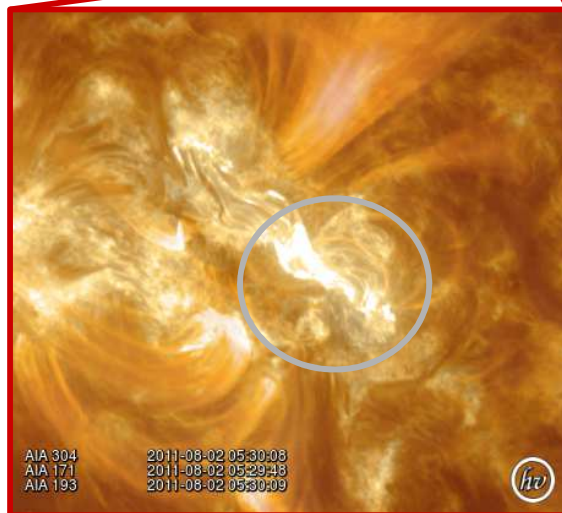
Temporal relation of flare-related EUV & X-ray emission

GOES SXR flux (0.5–8 Å)
GOES 1–8 Å derivative

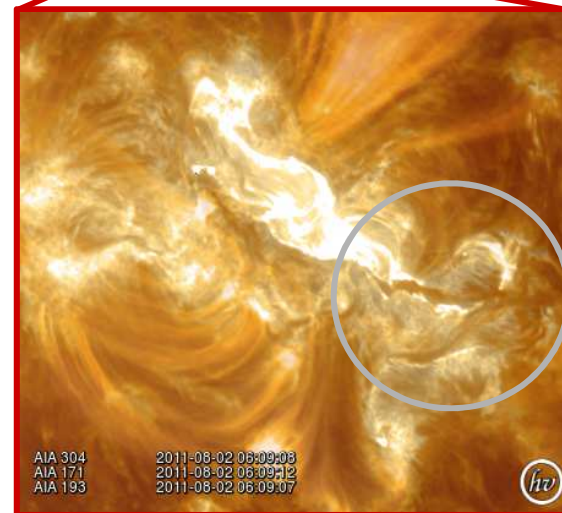


RHESSI count rates
— non-thermal
— thermal

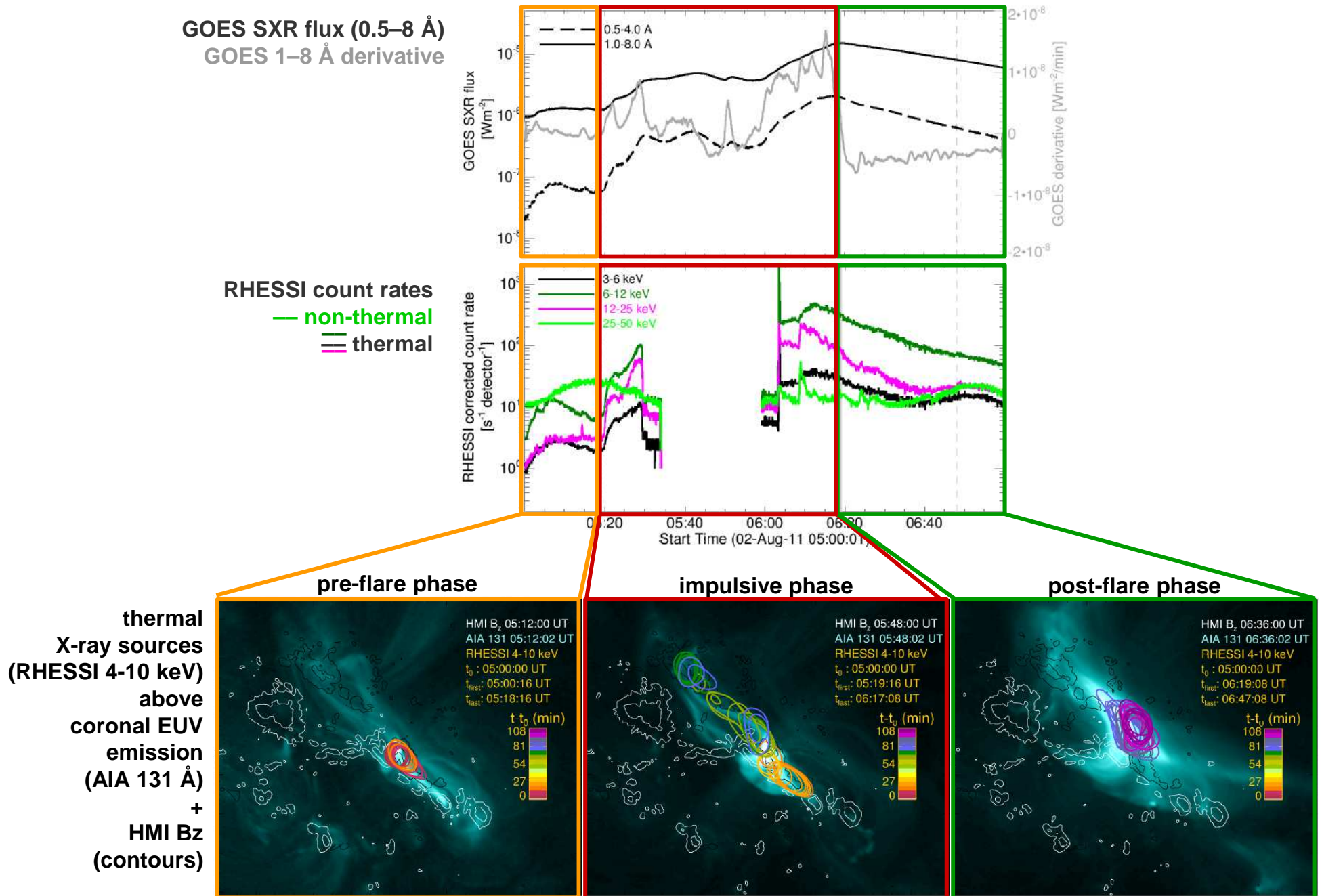
initiation of the flare process in a low-lying filament channel



partial filament eruption

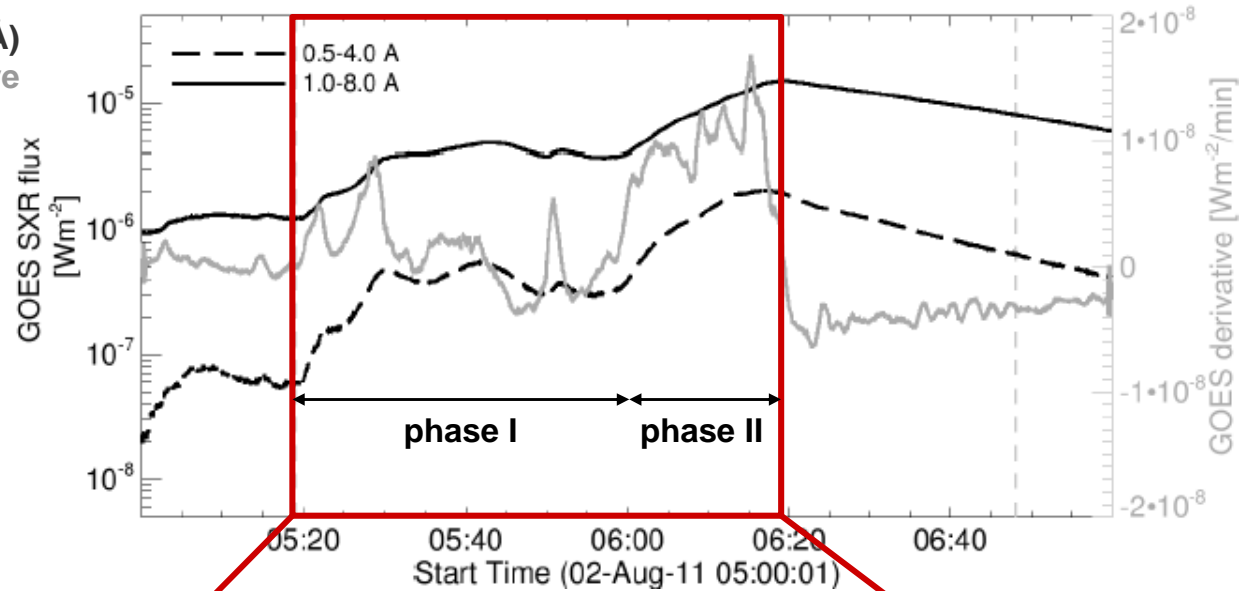


Spatial relation of flare-related EUV & X-ray emission

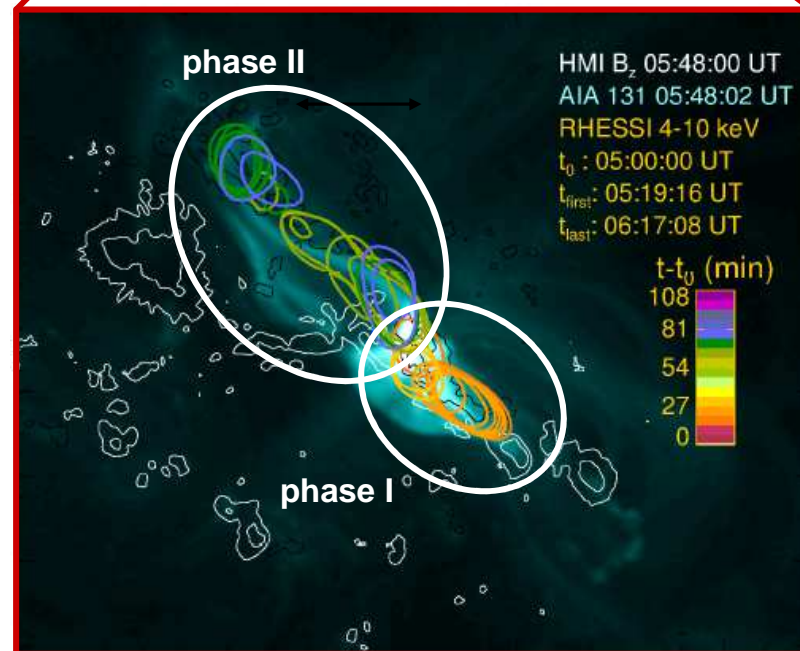


Spatial relation of flare-related X-ray & EUV emission

GOES SXR flux (0.5–8 Å)
GOES 1–8 Å derivative

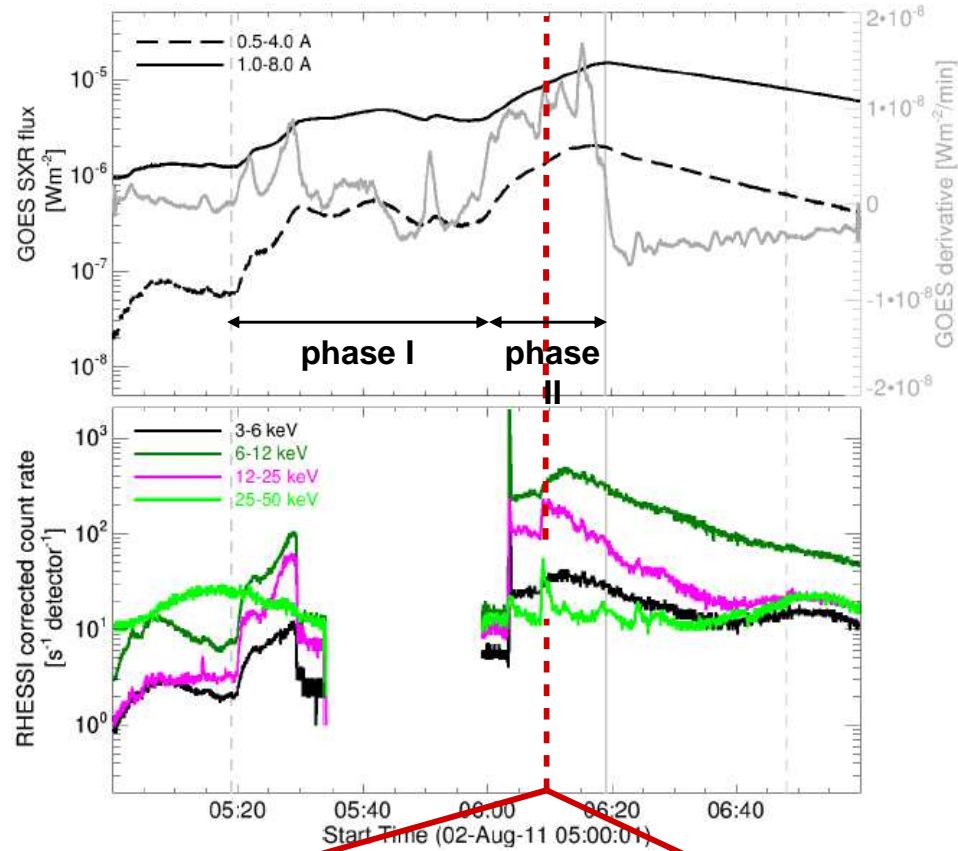


thermal
X-ray sources
(RHESSI 4-10 keV)
above
coronal EUV
emission
(AIA 131 Å)
+
HMI Bz
(contours)



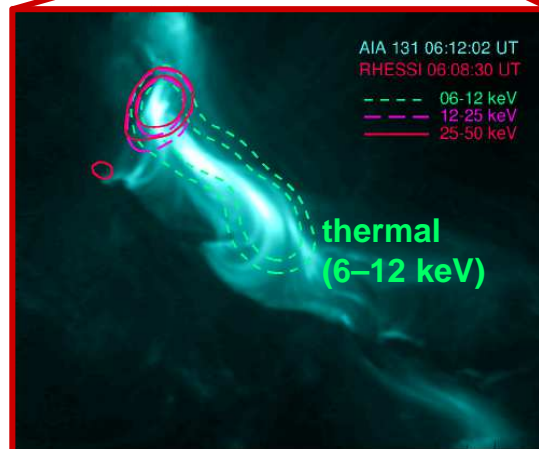
Spatial relation of flare-related X-ray & EUV emission

GOES SXR flux (0.5–8 Å)
GOES 1–8 Å derivative

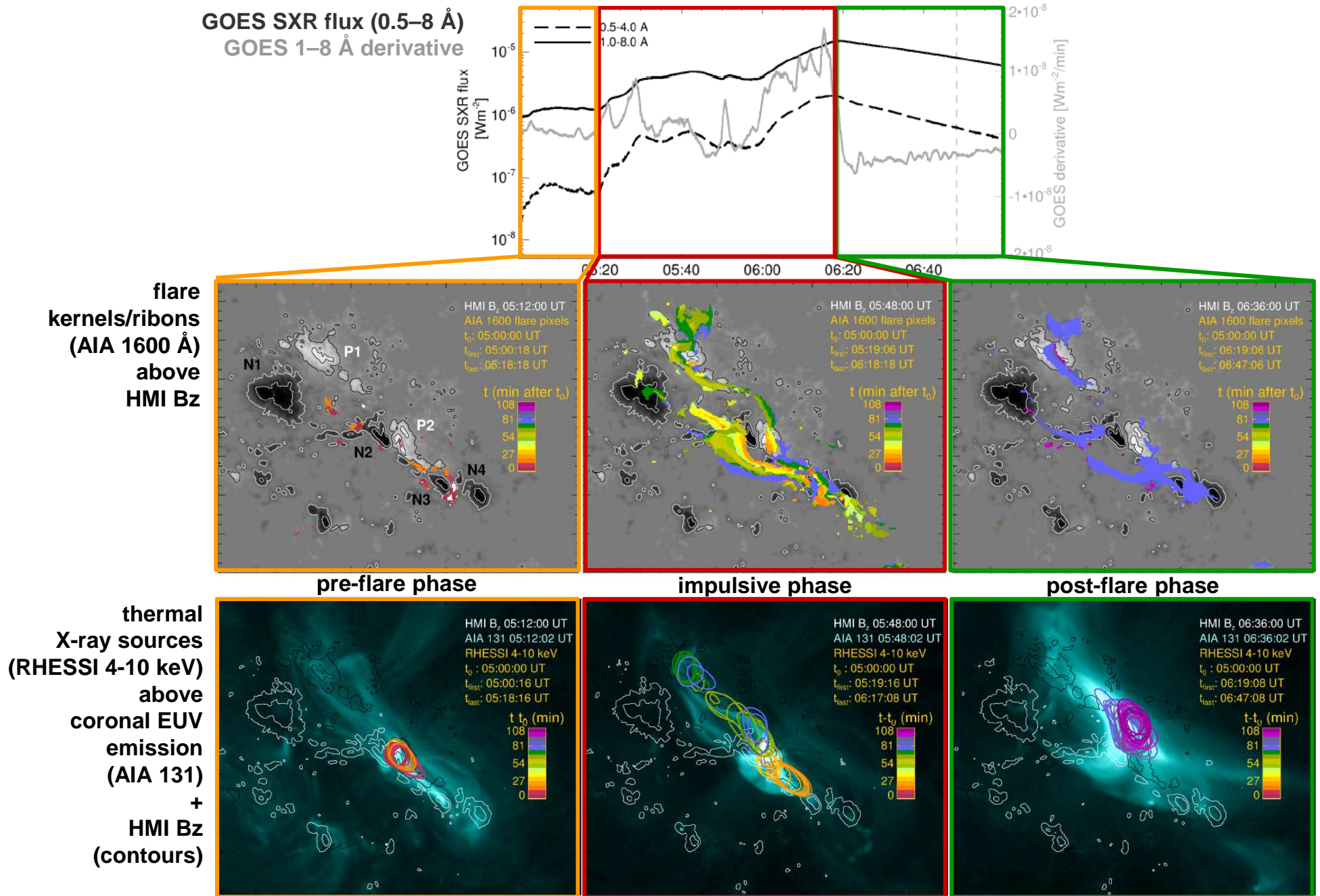


RHESSI count rates
— non-thermal
— thermal

non-thermal
X-ray sources
(RHESSI 12–25
and 25–50 keV)
above
coronal EUV
emission
(AIA 131 Å)

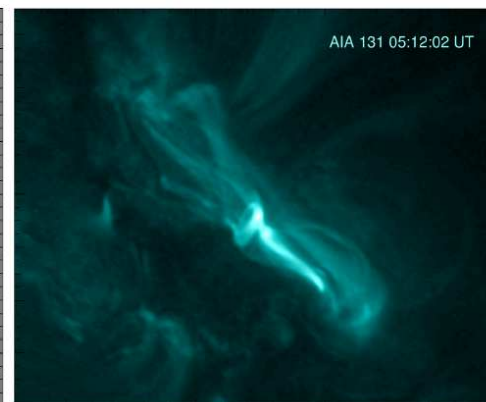
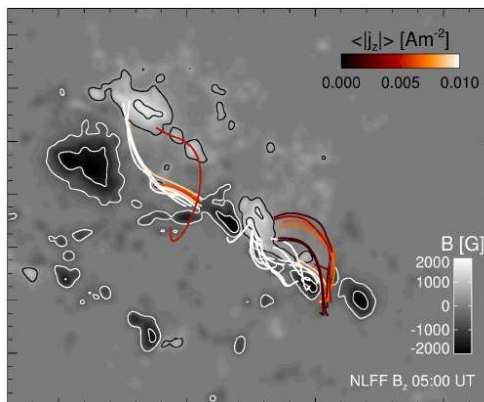
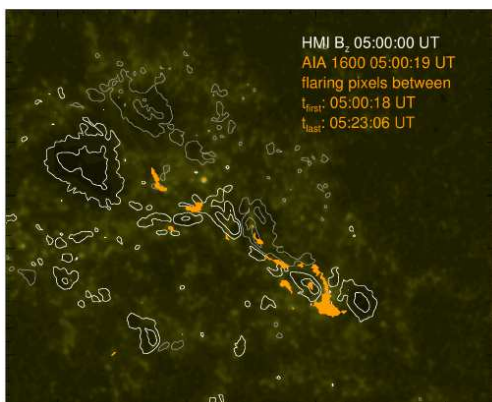


Spatial relation of flare-related UV & X-ray emission

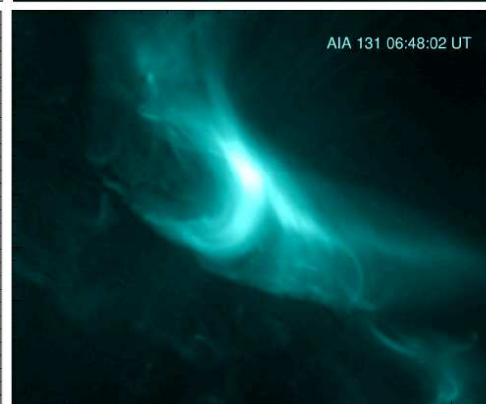
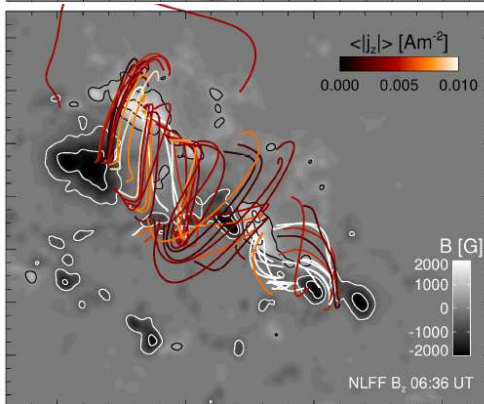
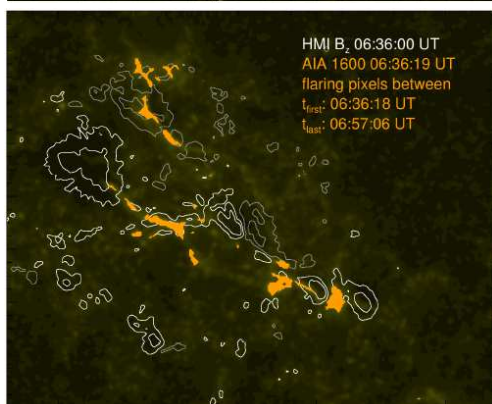
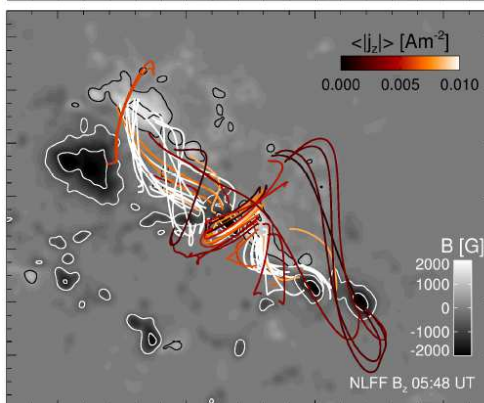
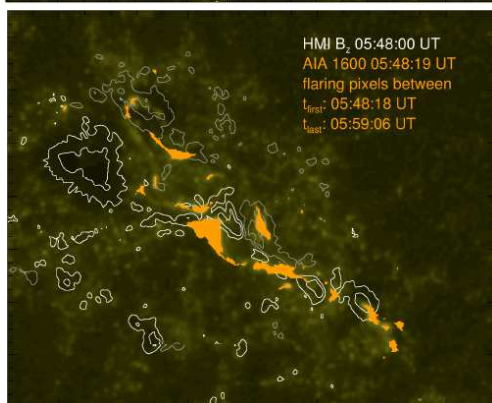


Relation of flare-related (E)UV emission & magnetic field

flare pixels
(12-minute
intervals)
above
AIA 1600 Å
+
HMI Bz
(contours)



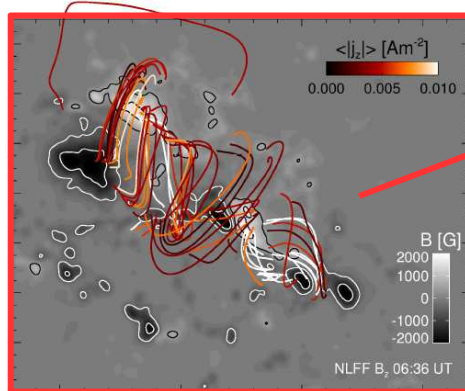
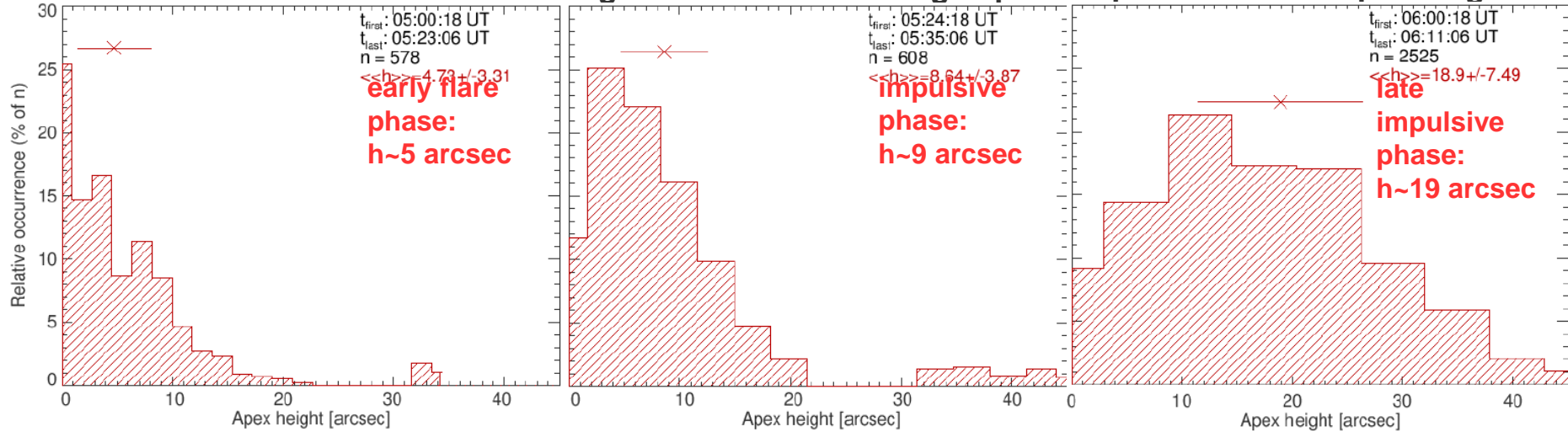
coronal
EUV
emission
(AIA 131 Å
at end of
12-min
intervals)



**NLFF (Wiegmann & Inhester, 2010, A&A, 516, A107)
model field lines (color code: mean vertical
current density at footpoints) above HMI Bz**

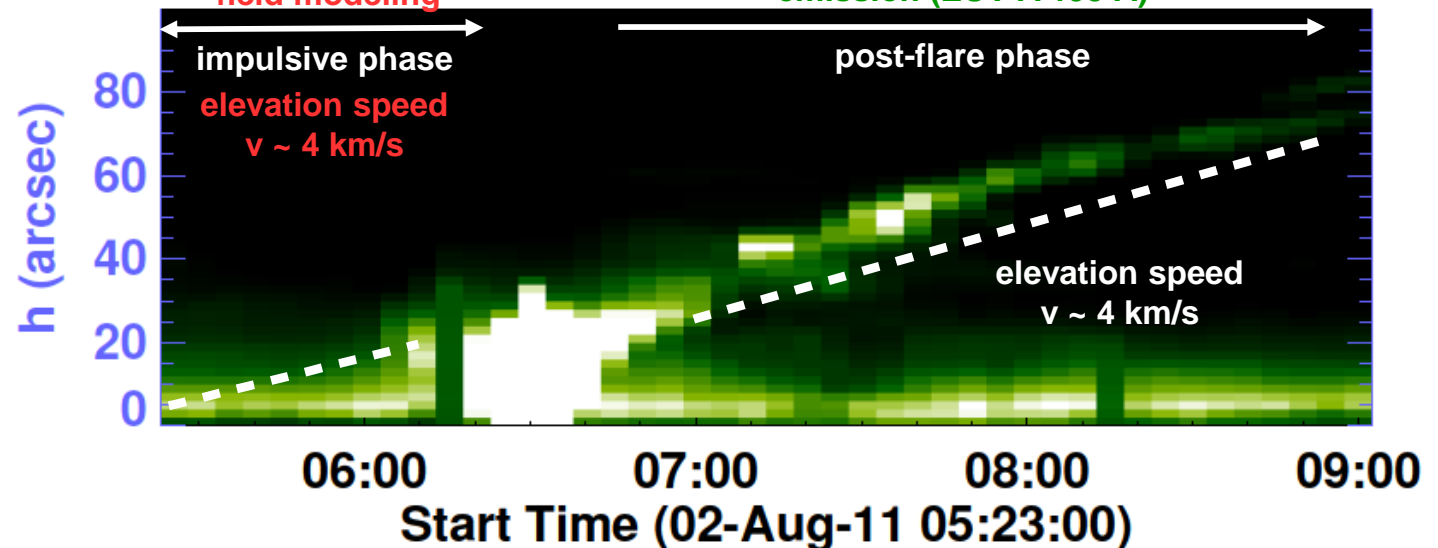
Approximate coronal height of reconnection region

statistics based on NLFF model magnetic field lines during impulsive phase: median apex height

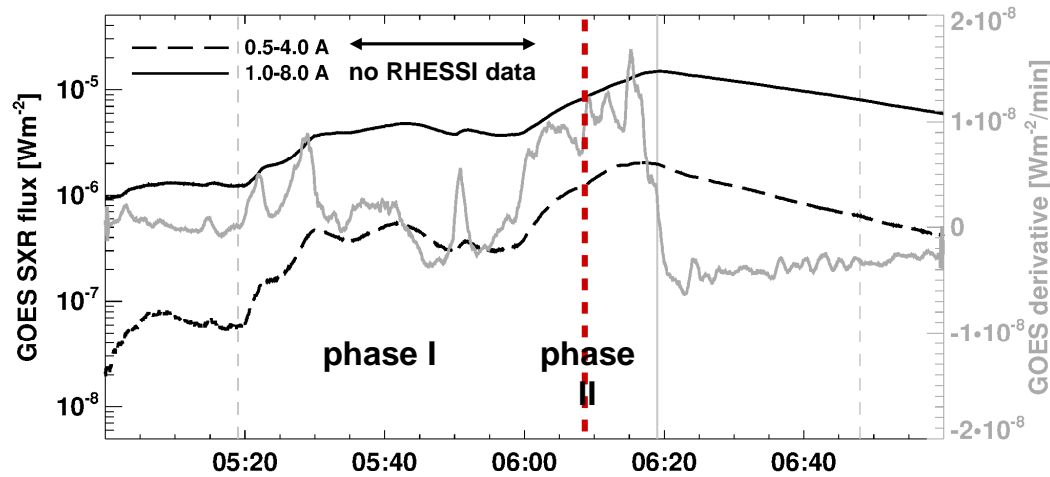


approximate altitude of coronal reconnection site derived from magnetic field modeling

derived from coronal EUV post-flare loop emission (EUV-A 195 Å)



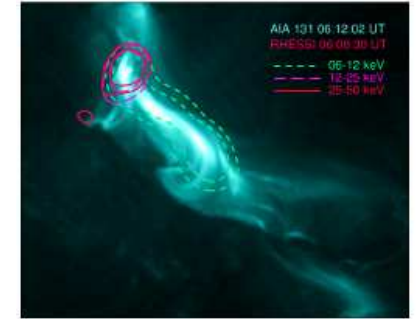
Summary (Thalmann, Su & Veronig, 2016, ApJ, accepted)



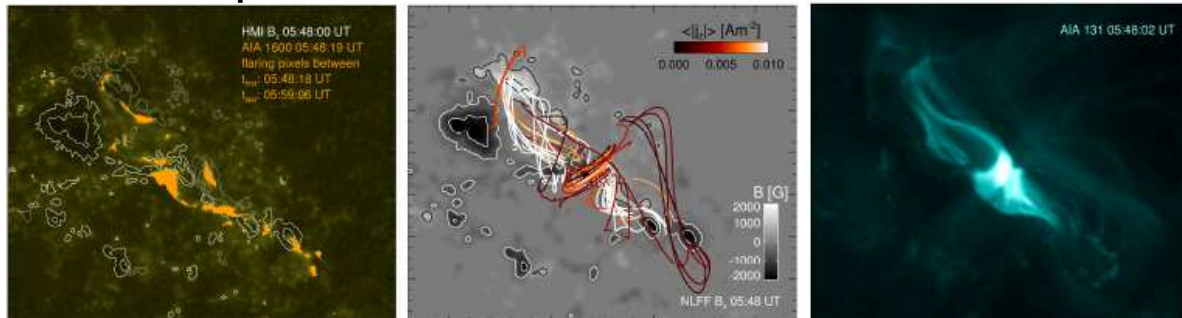
phase I
initiation of flaring process & partial filament eruption



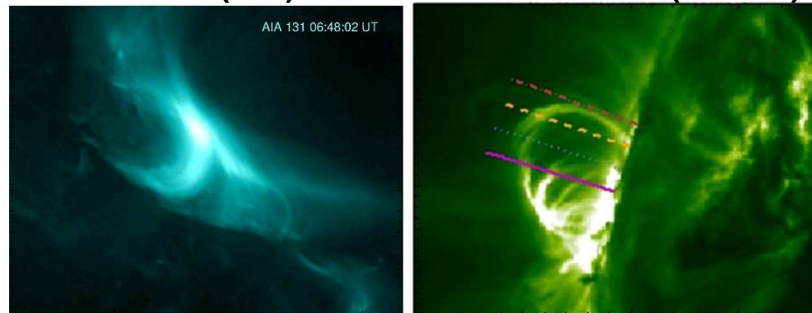
phase II
observation of HXR footpoint(s)



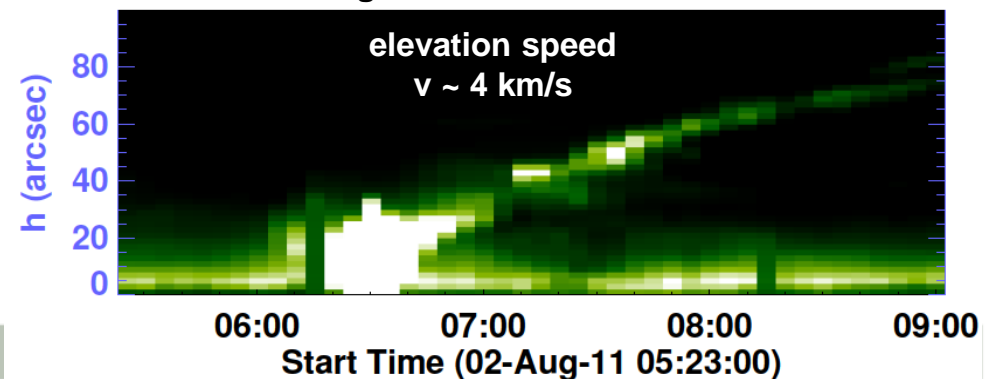
tracked flare pixels used as start locations for NLFF field line calculation



post-flare loops observed in coronal EUV images
on-disk (AIA) above the limb (EUVI-A)

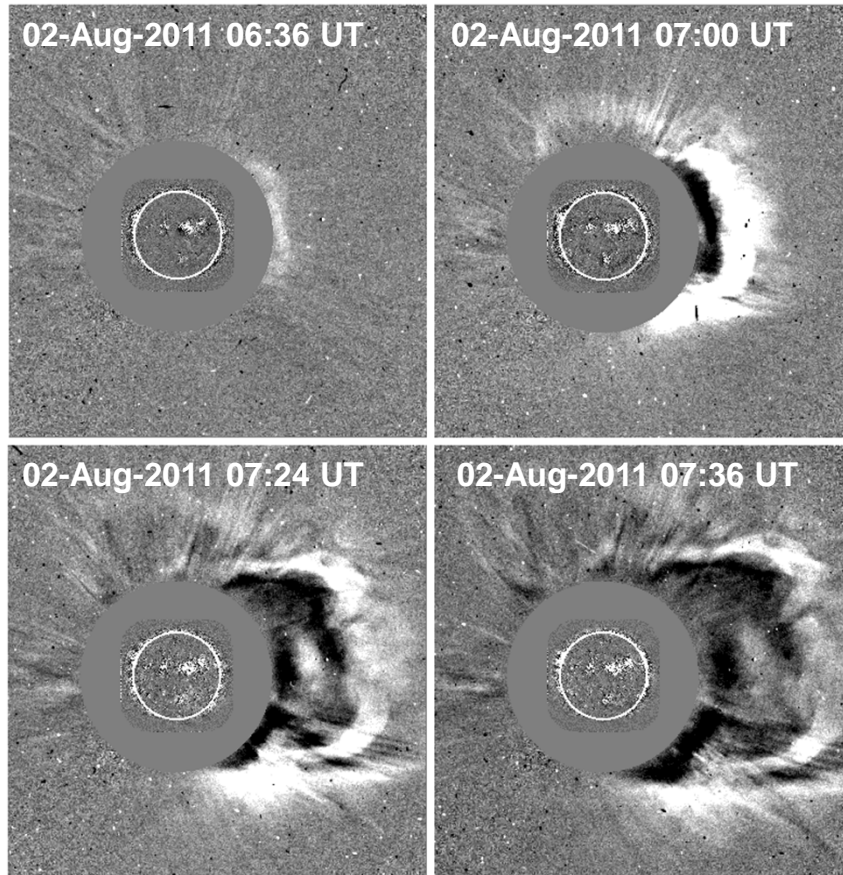


estimate of elevation speed of the coronal reconnection site
from magnetic field modeling from coronal observations observations



Coronal mass ejection & post-flare loop system

ejected plasma and magnetic flux
(LASCO-C2 white-light)



coronal EUV emission (EUVI-A 195 Å)

